Dynamics of Mode Competition in the Gyrotron Backward-Wave Oscillator

K. F. Pao,[1] T. H. Chang,[1] C. T. Fan,[1] S. H. Chen,[2] C. F. Yu,[1] and K. R. Chu[1]
[1]*Department of Physics, National Tsing Hua University, Hsinchu, Taiwan*
[2]*Department of Physics, National Changhua University of Education, Changhua, Taiwan*
(Received 3 June 2005; published 27 October 2005)

The axial modes of the gyrotron backward-wave oscillator (gyro-BWO) each exhibit a distinctive asymmetry in axial field profile. As a result, and in sharp contrast to the behavior of the familiar resonator-based gyrotron oscillator, particle simulations of the gyro-BWO reveal a radically different pattern of mode competition in which a fast-growing and well-established mode is subsequently suppressed by a later-starting mode with a more favorable field profile. This is verified in a Ka-band experiment and the interaction dynamics are elucidated with a time-frequency analysis.

DOI: 10.1103/PhysRevLett.95.185101 PACS numbers: 84.40.Ik, 84.40.Fe

The gyrotron backward-wave oscillator (gyro-BWO) is a continuously tunable source of coherent millimeter-wave radiation based on the electron cyclotron maser (ECM) interaction [1,2]. Oscillations build up in an internal feedback loop comprised of a forward moving electron beam and a backward propagating wave. The principle of the ECM was first demonstrated in backward-wave interactions [3]. Theoretical studies of the gyro-BWO first appeared in the mid-1960's in the Soviet literature (reviewed in Ref. [4]). Start-oscillation conditions and subsequent nonlinear behavior have been investigated in linear theories [5,6], orbit tracing calculations [7–16], and particle simulations [17]. Experimental gyro-BWO research [18–21] only began in earnest in the earlier 1990s and has generally been hampered by erratic behavior in frequency tuning. This, in large measure, accounts for the gyro-BWO's relatively unexploited status despite numerous applications which require continuously tunable sources.

The gyro-BWO interaction processes are distinctively different from those in the resonator-based gyrotron oscillator (gyromonotron). As illustrated later, the identities of the axial modes are determined by the electron dynamics [16] rather than by the interaction structure. In the nonlinear regime, the rf fields contract because of early depletion of the electron beam energy [12]. As a result, single-mode oscillations may remain stationary at beam currents (I_b) hundreds of times above the value at which the oscillation starts (I_{st}) [13–15]. However, the high threshold for single-mode nonstationary behavior does not preclude multimode competition at a much lower I_b when I_b exceeds the thresholds of two or more axial modes. This has been a concern not yet fully investigated, but is of critical importance to the stable operation of the gyro-BWO.

Axial modes and oscillation thresholds.—A weakly down-tapered waveguide interaction structure at the upstream end can more than double the interaction efficiency because of less abrupt electron bunching [11]. This is the practical configuration we have adopted for the present study of a 32–36 GHz, TE_{11}-mode gyro-BWO [Fig. 1(a)]. Because of the absence of cold resonant modes, field-shaping processes and the resultant axial field profile in a gyro-BWO depend entirely upon the beam-wave interaction. It was shown that the (hot) axial modes are characterized by a discrete set of optimum (linear) transit angles Θ separated by $\sim 2\pi$ [16], where Θ is the total wave phase variation observed by the electron in

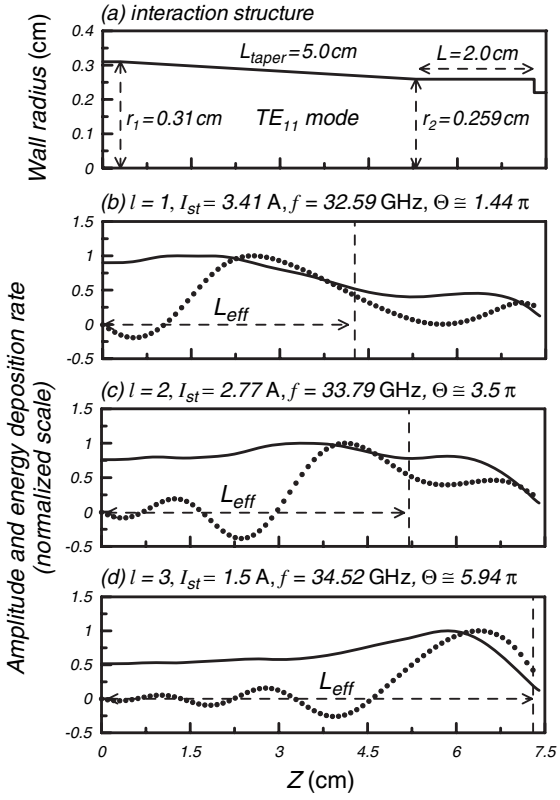

FIG. 1. (a) Shape and dimensions of the interaction structure. (b)–(d) Field amplitude (lines) and beam-energy deposition rate (dots) vs z for the first three axial modes at their respective I_{st} values. $V_b = 95$ kV, $v_\perp/v_z = 1.1$, r_c(guiding center position) = 0.09 cm, $\Delta v_z/v_z$(axial velocity spread) = 5%, and B_0 = 14.8 kG. (= 1.32 times the left-end grazing field and 1.11 times the right-end grazing field).

traversing the interaction space. This is borne out in Figs. 1(b)–1(d) which display the field amplitude and beam-energy deposition profiles for the first three axial modes ($l = 1$–3) at their respective I_{st} values. The results are based on a single-mode, steady-state code [22] and relevant parameters are given in the figure and figure caption. Regions to the right of the vertical dashed lines are cut off from the oscillation frequency; hence, the transit angle is defined with respect to the effective interaction length (L_{eff});, namely, the length to the left of the dashed line. The field amplitude always begins with an initial absorption dip [1]. Each increase in the mode index is accompanied by a step increase in Θ, which results in one more region of negative energy deposition and an additional trough of the field amplitude. The energy deposition profiles thus give each axial mode a distinctive asymmetry in field distribution.

There are two opposing factors which influence the I_{st} value for the tapered interaction structure under study. Higher-order modes have a higher frequency and hence a longer L_{eff}, which lowers I_{st}. On the other hand, they also have a larger Θ and hence weaker interaction strength, which raises I_{st}. At $B_0 = 14.8$ kG, the former factor plays the major role for the $l = 1$–3 modes. Thus, as shown in Fig. 1, the I_{st} value decreases with l. However, the latter factor dominates for the $l > 3$ modes, resulting in I_{st} values greater than those of the $l = 1$–3 modes.

Dynamics of axial mode competition and physical interpretation.—The existence of multiple axial modes (in particular, a higher-order mode with a lower I_{st}) raises the important question as to how they interact when two or more modes are excited. Here, we attempt to resolve this issue both theoretically and experimentally. A time-dependent, particle-in-cell code is employed to follow the evolution of the axial modes. A time-frequency analysis [23,24] is then performed on the ac output signal. For later comparison with the experiment, we use the experimental beam voltage/current pulse shapes and the corresponding $v_\perp/v_z$ (Fig. 2).

A two-mode competition process is illustrated in Fig. 3 for I_b(peak) = 4.2 A and a fixed magnetic field of 14.8 kG,

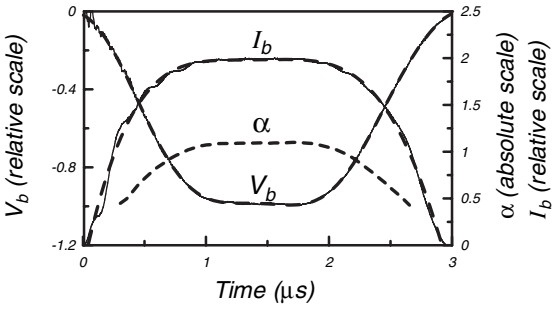

FIG. 2. Experimental voltage and current traces (thin lines) and their polynomial fits (dashed curves) used for the simulation. The α curve is based on electron gun simulations.

for which $I_{st} = 3.36$, 2.72, and 1.46 A for $l = 1$, 2, and 3, respectively, (see Fig. 1). A brief stage of mode competition is seen early in the beam pulse [Fig. 3(a)], the details of which are evident from the time-dependent spectrum [Fig. 3(b)] of the output signal. In spite of a lower growth rate, the lower-order $l = 2$ mode rapidly suppresses the higher-order $l = 3$ mode and it persists till the end of the beam pulse where the $l = 3$ mode interaction, with a comparable I_{st}, becomes too weak to be reexcited. In this and the following figures, the frequency of a given mode varies during the rise and fall of the beam pulse so that the transit angle remains at the optimum value for the mode. A three-mode competition sequence takes place at an increased I_b, as is illustrated in Fig. 4 for I_b(peak) = 4.8 A. During the rise time of the beam pulse (cf. Figure 2), the $l = 3$ mode first emerges [Fig. 4(b)] and is immediately suppressed by the $l = 2$ mode, which in turn is suppressed by the lowest-order and latest-start $l = 1$ mode as the beam pulse flattens. The $l = 1$ mode remains dominant over the flat portion of the pulse until I_b falls below its threshold. Then, the competition between the $l = 2$ and 3 modes resumes in the same manner as during the rise time, thereby exhibiting a hysteresis effect. Hysteresis effects have also been observed in the BWO under different conditions [25].

These sequences of mode competition exhibit a consistent pattern in which a fast-growing and well-established mode is subsequently suppressed by a later-starting, lower-order mode. This can be explained by the intrinsic asymmetry of the axial mode profiles. As shown in Fig. 1, a lower-order mode has a field peak closer to the beam

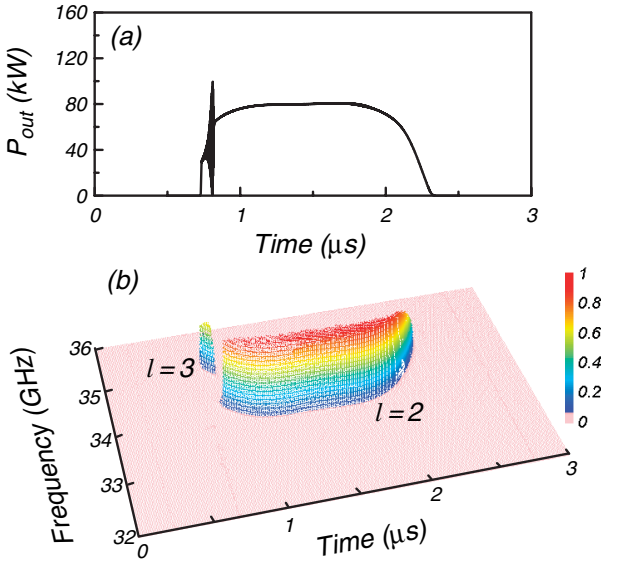

FIG. 3 (color). (a) Simulated output power (P_{out}) vs time. (b) Time-dependent frequency spectrum of the output signal (amplitude in color code). V_b, I_b, and α profiles are shown in Fig. 2. I_b(peak) = 4.2 A and other parameters are the same as in Fig. 1.

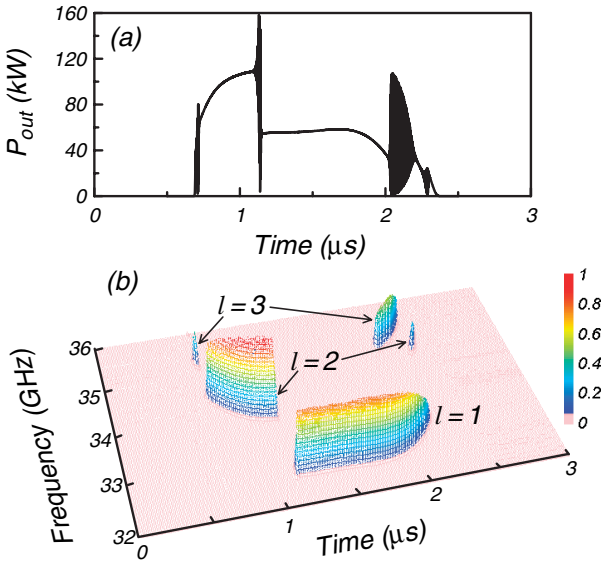

FIG. 4 (color). Same plots as in Fig. 3 for an increased beam current of I_b(peak) = 4.8 A.

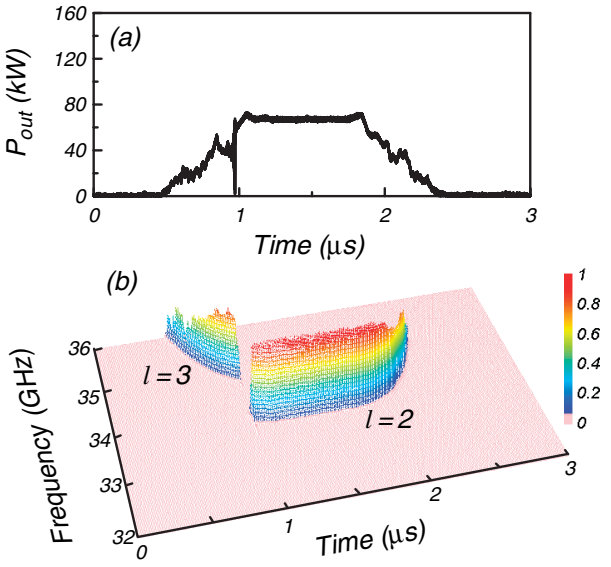

FIG. 5 (color). (a) Measured P_{out} vs time. (b) Time-dependent frequency spectrum of the output signal. I_b(peak) = 4.18 A (see Fig. 2) and other parameters are the same as in Fig. 1.

entrance and hence the advantage of early interaction with the beam. As the lower-order mode grows to a significant amplitude, the self-consistent beam perturbations associated with this mode would appear as deleterious momentum-energy spreads to the other modes and consequently result in their suppression. This also explains why the $l = 1$ mode, with the lowest I_{st}, will always be the dominant mode in a uniform waveguide. We note that, although Figs. 3 and 4 were obtained for a pulsed beam (Fig. 2), the same effects have been observed in constant V_b and I_b simulations.

Experimental verification.—The basic experimental setup was described in Ref. [13]. At the upstream end, the ac output signal was mixed with a 32 GHz local oscillator signal for the time-dependent spectral analysis, while the output power was measured with a calibrated crystal detector with an estimated accuracy of ±5% at the frequency of the dominant mode.

Except for minor quantitative differences, the experiments at I_b(peak) = 4.18 A and 4.88 A yielded the same results as shown in Figs. 3 and 4, respectively. The temporal traces of the output power [Figs. 5(a) and 6(a)] and the time-dependent frequency spectrum [Figs. 5(b) and 6(b)] reproduce the essential features of the simulated behavior in Figs. 3 and 4, including the time duration of mode competition and the order of mode transition.

Further examination at different beam currents.—As shown in Figs. 3–6, axial mode competition is characterized by the eventual dominance of the lowest-order competing mode. Figure 7 shows the simulated (lines) and observed (circles) dominant mode as a function of the peak I_b. The dominant mode is seen to always transition down to a lower-order mode at a sufficiently high I_b value. In the simulation, the $l = 3$ mode appears first as I_b rises. Its efficiency increases with I_b to the value of ~21.9% in single-mode operation until $I_b = 3.7$ A (1.36 times I_{st} of the $l = 2$ mode), beyond which it transitions to the $l = 2$ mode, which subsequently transitions to the $l = 1$ mode at $I_b = 4.4$ A (1.31 times I_{st} of the $l = 1$ mode). The experimental data show a consistent trend, but the transition occurs at a somewhat different current. Each transition in Fig. 7 is preceded by a narrow range in I_b (~0.2 A in simulation and significantly narrower in experiment) in which mode competition persists throughout the beam pulse.

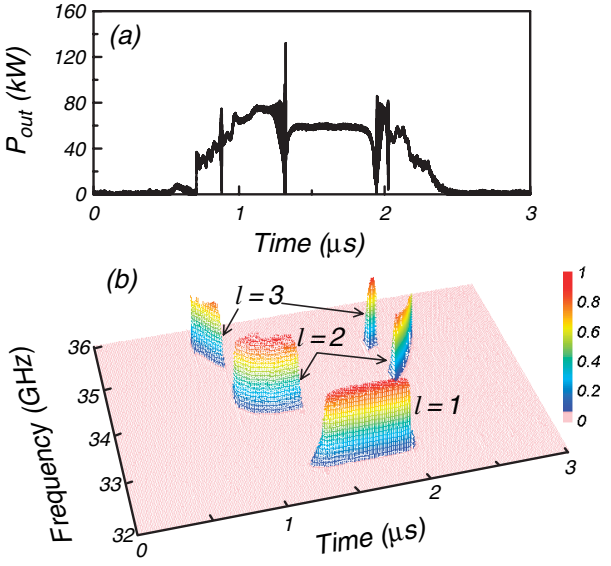

FIG. 6 (color). Same plots as in Fig. 5 for an increased beam current of I_b(peak) = 4.88 A.

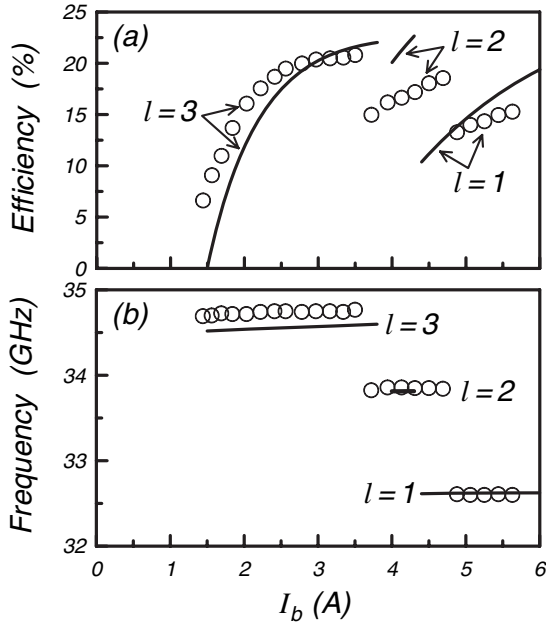

FIG. 7. Simulated (lines) and measured (circles) interaction efficiency and oscillation frequency of the dominant mode vs I_b for the parameters given in Fig. 1.

In summary, theoretical and experimental investigations have elucidated the governing mechanisms of axial mode competition in the gyro-BWO. Results indicate that the asymmetry of the axial field profile, rather than the growth rate or the start-oscillation current, determines the competitiveness of a specific mode. At a beam current sufficiently above its threshold, a lower-order mode with a more favorable field profile will suppress a faster-growing and well-established higher-order mode. This is a scenario fundamentally different from that of the gyromonotron, where the first excited mode tends to suppress all other modes [26,27]. Also, in contrast to the persistent nature of the single-mode nonstationary behavior in the gyromonotron and gyro-BWO [14–16], the multimode nonstationary behavior is generally characterized by a brief stage of mode competition, followed by the stationary oscillation of the lowest-order mode in the competition. These insights are expected to provide a new perspective for the understanding of the diverse nonstationary behavior in gyro-devices.

This work was supported by the National Science Council, Taiwan. The authors are grateful to Professor N. C. Luhmann, Jr. and Dr. L. R. Barnett for their critical comments.

[1] K. R. Chu, Rev. Mod. Phys. **76**, 489 (2004).
[2] G. S. Nusinovich, *Introduction to the Physics of Gyrotrons* (John Hopkins University Press, Maryland, 2004).
[3] R. H. Pantell, Proc. IRE **47**, 1146 (1959).
[4] G. S. Nusinovich and O. Dumbrajs, IEEE Trans. Plasma Sci. **24**, 620 (1996).
[5] S. Y. Park, V. L. Granatstein, and R. K. Parker, Int. J. Electron. **57**, 1109 (1984).
[6] C. S. Kou, Phys. Plasmas **1**, 3093 (1994).
[7] V. K. Yulpatov, Radiophys. Quantum Electron. **10**, 471 (1967).
[8] N. S. Ginzburg, I. G. Zarnitsyna, and G. S. Nusinovich, Radio Eng. Electron. Phys. **24**, 113 (1979).
[9] V. L. Bratman, N. S. Ginzburg, G. S. Nusinovich, M. I. Petelin, and P. S. Strelkov, Int. J. Electron. **51**, 541 (1981).
[10] A. K. Ganguly and S. Ahn, Appl. Phys. Lett. **54**, 514 (1989).
[11] C. S. Kou, C. H. Chen, and T. J. Wu, Phys. Rev. E **57**, 7162 (1998).
[12] S. H. Chen, K. R. Chu, and T. H. Chang, Phys. Rev. Lett. **85**, 2633 (2000).
[13] T. H. Chang, S. H. Chen, L. R. Barnett, and K. R. Chu, Phys. Rev. Lett. **87**, 064802 (2001).
[14] G. S. Nusinovich, A. N. Vlasov, and T. M. Antonsen, Jr., Phys. Rev. Lett. **87**, 218301 (2001).
[15] A. Grudiev and K. Schunemann, IEEE Trans. Plasma Sci. **30**, 851 (2002).
[16] S. H. Chen, T. H. Chang, K. F. Pao, C. T. Fan, and K. R. Chu, Phys. Rev. Lett. **89**, 268303 (2002).
[17] A. T. Lin, Phys. Rev. A **46**, R4516 (1992).
[18] S. Y. Park, R. H. Kyser, C. M. Armstrong, R. K .Parker and V. L. Granatstein, IEEE Trans. Plasma Sci. **18**, 321 (1990).
[19] C. S. Kou, S. H. Chen, L. R. Barnett, H. Y. Chen, and K. R. Chu, Phys. Rev. Lett. **70**, 924 (1993).
[20] M. A. Basten, W. C. Guss, K. E. Kreischer, R. J. Temkin, and M. Caplan, Int. J. Infrared Millim. Waves **16**, 889 (1995).
[21] W. He, A. W. Cross, C. G. Whyte, A. R. Young, A. D. R. Phelps, K. Ronald, E. G. Rafferty, J. Thomson, C. W. Robertson, D. C. Speirs, S. V. Samsonov, V. L. Bratman, and G. G. Denisov, *Proceedings of the 29th International Conference on Infrared and Millimeter Waves*, edited by M. Thumm and W. Wiesbeck (IEEE, New York, 2004), p. 235.
[22] K. R. Chu, H. Y. Chen, C. L. Hung, T. H. Chang, L. R. Barnett, S. H. Chen, T. T. Yang, and D. Dialetis, IEEE Trans. Plasma Sci. **27**, 391 (1999).
[23] B. Boashash, *Time-Frequency Signal Analysis* (Halsted Press, New York, 1992).
[24] C. W. Peters, R. L. Jaynes, Y. Y. Lau, R. M. Gilgenbach, W. J. Williams, J. M. Hochman, W. E. Cohen, J. I. Rintamaki, D. E. Vollers, and T. A. Spencer, Phys. Rev. E **58**, 6880 (1998).
[25] G. S. Nusinovich and Yu. P. Bliokh, Phys. Plasmas **7**, 1294 (2000).
[26] G. S. Nusinovich, IEEE Trans. Plasma Sci. **27**, 313 (1999).
[27] K. E. Kreischer and R. J. Temkin, Phys. Rev. Lett. **59**, 547 (1987).